Laser Parameter Study on Cutting Metal using CO2 Laser

Dongkyoung Lee (ldkkinka@kongju.ac.kr)
Kongju National University, Cheonan, South Korea

Research Article

Keywords: High-power laser cutting, laser parameters, cutting quality

Posted Date: October 30th, 2020

DOI: https://doi.org/10.21203/rs.3.rs-98836/v1

laser parameter study on cutting metal using CO2 laser

Seungik Son[1], Dongkyoung Lee[1*]

[1]Department of Mechanical and Automotive Engineering, Kongju National University, Cheonan, South Korea

Abstract

This experimental study investigated for the effect of laser parameters on machining of the SS41 and SUS304. These materials play an importance role in engineering aspect. They are widely used in high-tech industries such as aerospace, automotive, and semiconductor. Due to the development of technology and high-tech industrialization, the various processing technologies requiring high precision are being developed. However, the conventional cutting process is difficult to meet high precision processing. Therefore, to achieve high precision processing of the SS41 and SUS304, laser manufacturing has been applied. The experiment investigates the process quality of laser cutting for SS41 and SUS304, with the usage of a continuous wave CO_2 laser cutting system. The experimental variables are set to the laser cutting speed, laser power, and different used materials. The results are significantly affected by the laser parameters. As the results, the process quality of the laser cutting has been observed by measuring the top and bottom kerf widths, as well as the size of the melting zone and HAZ according to E_{line}. In addition, the evaluation of the laser processing parameters is significantly important to achieve optimal cutting quality. Therefore, we observed the correlation between the laser parameters and cutting quality. These were evaluated by analysis of variance (ANOVA) and multiple regression analysis.

Keywords: High-power laser cutting, laser parameters, cutting quality

[1] Corresponding Author at: Department of Mechanical and Automotive Engineering, Kongju National University, Cheonan, South Korea

Tel: +82 41 521 9260; Fax: +82 41 555 9123

Email address: ldkkinka@kongju.ac.kr

1. Introduction

SS41 is a structural steel containing Si and Mn. It is widely used in various fields such as aerospace, automobiles, ships, and construction due to its low cost. SUS304 has high corrosion resistance due to containing Cr component. These metallic materials characterize with low thermal deformation therefore, it is generally used for various applications without surface treatment. However, it is challenging issue to machine SS41 and SUS304 with high precision processing using conventional technique. Thus, the manufacturer prefers to use high-power laser processing rather than mechanical processing. Besides, it is supported to conventional machining in order to improve machinability. The laser processing has more advantages than mechanical processing. Laser machining can be performed on various materials, without tool wear and additional cost. The method is non-contact processing, which provides flexibility in processing. [1-14]. The manufacturers using high-power laser processing are concerned for the optimize the quality and productivity of the products. However, to improve product quality and productivity, the effects of laser parameters on the material should be considered as major issue. In addition, in order to control the influence of the laser beam, the laser parameters must be selected appropriately. Indeed, adjustable laser parameters include laser power, cutting speed, assist gas pressure and stand-off distance.

To maintain high precision and good quality process, the laser parameters applied to the process should be properly selected, but the effect of the parameters is difficult to predict. Besides, many manufacturers spend a lot of time and effort to determine the laser parameter which is suitable to apply for the process. In the previous studies, experiments were carried out according to specific laser parameters, and there was a comparative analysis of the effect of each parameter on the processing quality. Lamikiz et.al.[15] suggested the optimum working areas and cutting conditions

for the laser cutting of steel. The main experimental parameter was the thickness of the material and the results showed a remarkable different behavior between the thinnest and the thickest sheets. H.Kaebernick et.al.[16] described a monitoring technique in laser cutting. The analytical techniques prove that the surface roughness was improved by controlling laser pulses. N.Rajaram et. al.[17] studied the effect of parameters on the characteristics of steel specimens. The material was cut through a CO_2 laser cutting system, and cutting results were analyzed with kerf width, surface roughness, and Heat affected zone size. The material which was cut using the CO_2 laser showed the different results depending on the change of parameters. B S Yilbas [18] suggests that various parameters are affected during the laser cutting process and then, the laser power and the cutting speed for the kerf width are examined. It is confirmed that the kerf width increases with the combination of the laser power and the energy coupling factor. Cristina Anghel et.al.[19] demonstrates the experiment of laser cutting on 304 stainless steel miniature gear. In the experiment, The CO2 laser system was employed to cut the miniature. The effects of laser parameters on average surface roughness (Ra) has been investigated the surface of craters and cracks.

In the previous studies have done significant investigation on the influence of laser parameters in laser cutting process to the materials. However, it is determined that not only the influence of each parameter but also the interaction between the parameters can affect the high - power laser processing for the different metallic materials. Therefore, this study predicted and analyzed the effect of high-power laser parameters on the different metallic materials. Multiple regression and analysis of variance (ANOVA) are used to predict the kerf width, melting width, and heat affected zones generated after laser cutting. In addition, these are used to investigate the effects of parameter and interaction between parameters.

2. Experimental set up

In the present study, a continuous wavelength CO_2 laser was used for the cutting process. During the experiment, the stand-off distance of the laser is constant, and the nozzle size is fixed at 0.2 mm. In addition, assistance gas is used by the constant pressure of N_2 and O_2 to maintain high processing quality. Table 1 shows the laser parameters applied to SS41 and SUS304. Different laser powers and cutting speeds were conducted to cut the materials in the experiment. In the parameters applied to the experiments, if they are outside the set range, each material was not cut. Therefore, the parameters shown in Table 1 are applied for laser cutting process. Table 2 shows the chemical composition of the materials used in the experiment. In order to analyze the experimental results, the kerf widths generated after cutting process are measured on both top and bottom surface. In addition, melting width and heat affected zone formed in the bottom surface of the materials are measured.

	Steel	SuS304
Laser Power	1000-3700	2100-3900
Cutting speed	2000-4100	2000-3500
Assistance gas	N_2	O_2
Gas pressure	3	3
Thickness	2	2

Table 1 Laser parameter

SS41	C	Si	Mn	P	S
Properties [%]	0.14~0.22	≤ 0.3	0.36~0.65	≤ 0.045	≤ 0.05

SUS304	C	Si	Mn	P	S	Ni	Cr
Properties [%]	0.08	1.00	2.00	0.45	0.30	8.00~10.50	18.00~20.00

Table 2 Materials properties

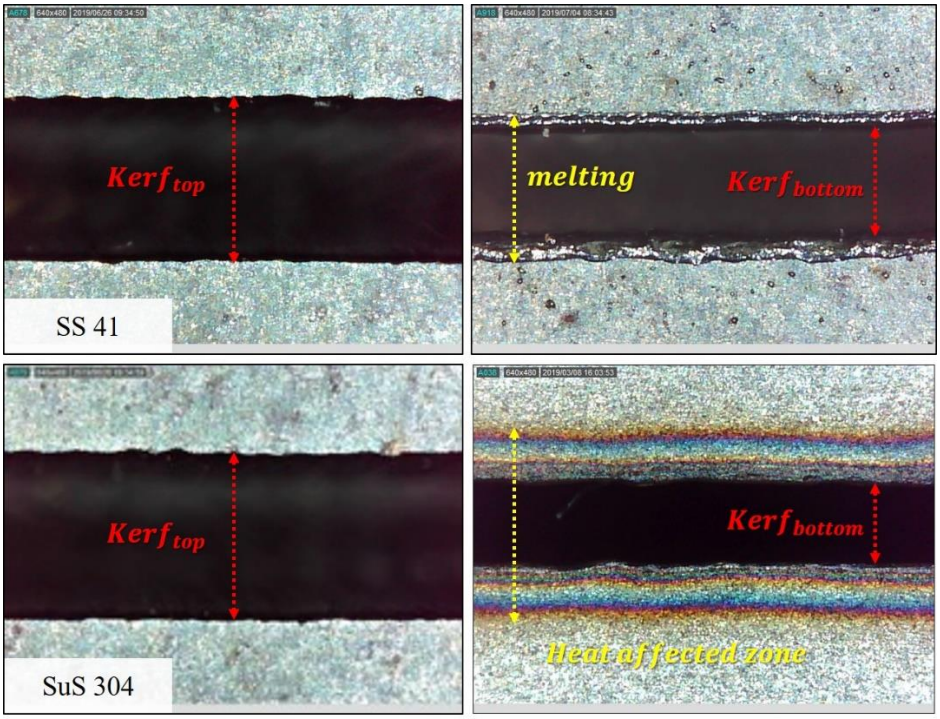

Figure 1 Measurement method

3. Result and discussion

Line energy is a parameter which represents the irradiated laser per unit volume, and it is equals by the laser power divided by the laser scanning speed and the laser beam size. Line energy is

also an important parameter in the laser cutting process which demonstrates material removal mechanisms and to evaluates laser cutting efficiency [20].

$$E_{line} = \frac{P_{laser}}{Vs*A} \ (J/m^3) \ (1)$$

where, P_{laser} is the laser power, V_s is the cutting speed, A is the spot size of the laser beam. Experimental results are analyzed through E_{line} to identify the effect on the laser powers and cutting speed that changed during the experiment.

3.1 Analysis of kerf width in SS41 according to E_{line}

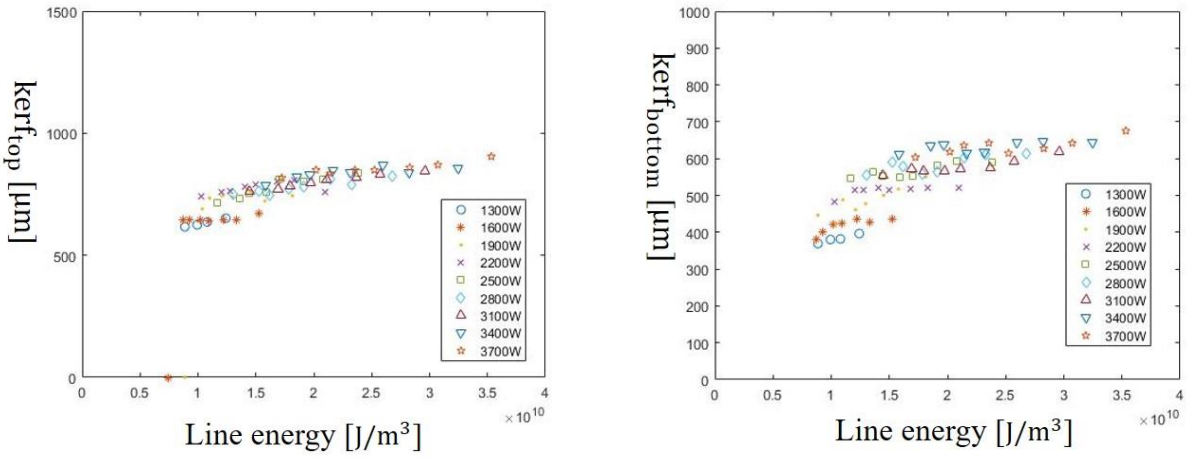

Figure 2 Variation of $\boldsymbol{kerf_{top}}$ *and* $\boldsymbol{kerf_{bottom}}$ *according to* $\boldsymbol{E_{line}}$

The effect of E_{line} on the kerf width of SS 41 is shown in Figure 2. The measurements of the kerf widths are conducted on both top and bottom sections of the cutting material. The graph indicates a visible trend of an increase of the kerf widths in function of line energy. The kerf widths

on top are slightly larger than bottom surface. This happen due to various reasons, such as loss of intensity of the beam, defocusing of the laser beam, or loss of gas pressure. In Figure 2, each kerf width is observed with higher values as the E_{line} increases. At the laser power of 3700W, kerf top and kerf bottom are observed with the highest widths of 905 µm and 675 µm, respectively. In the interaction between laser and materials, it is evident that kerf width is affected by cutting speed. With lower cutting speed, the material is heated until it evaporates rapidly and removed material easily on the top surface. Therefore, the wider kerf widths are formed on the top surface. Besides, when laser power increases, E_{line} also increases. As the results, the kerf widths increase because the increasing energy line causes significant influence on the material.

3.2 Analysis of melting width in SS41 according to E_{line}

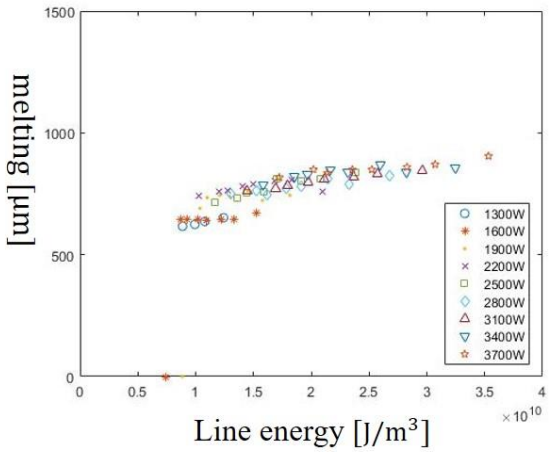

Figure 3 Variation of melting according to $\boldsymbol{E_{line}}$

The results from the melting width measurements are shown in Figure 3. Each measured data in this result is obtained with measuring averaging melting width. Melting is the area where the material melts due to the laser irradiation and it occurs around the kerf width. At most of the laser powers set in the experiment, melting width increases with increasing E_{line}. The melting width is the maximum melting width is obtained in the process with laser power of 3700W. In short, the laser beam including the laser power and cutting speed directly affect the material. E_{line} is proportional to laser power, and as the laser power increases, the E_{line} energy affecting with material increase. However, in the case of cutting speed, as the cutting speed decreases, the thermal energy entering the material increases. As a result, melting width increases as E_{line} increases.

3.3 Analysis of kerf width in SUS304 according to E_{line}

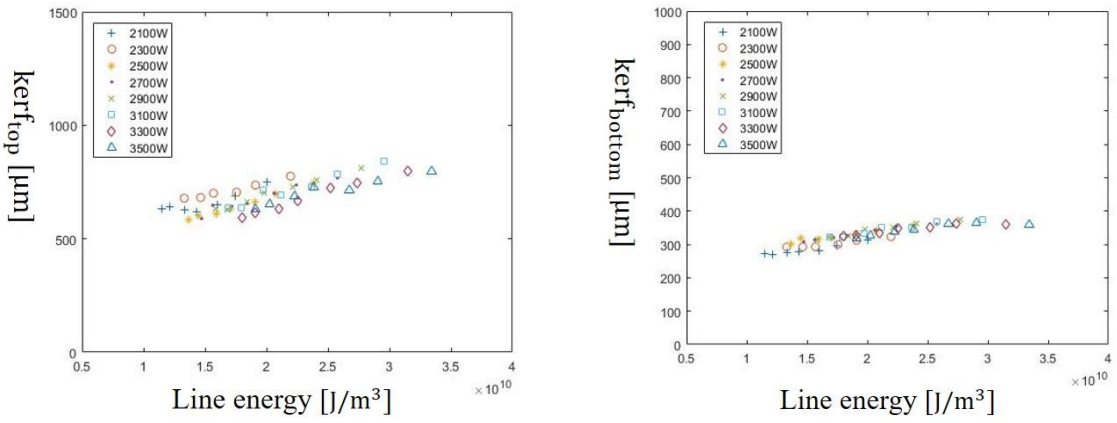

Figure 4 variation of $\boldsymbol{kerf_{top}}$ and $\boldsymbol{kerf_{bottom}}$ in SUS304 according to E

The effects of E_{line} on the kerf width of SUS304 is shown in Figure 4. The measurement of kerf width on SUS304 is performed in the same method as that on SS 41. In kerf widths on E_{line},

there is a similar trend, except that the kerf top is larger than the kerf bottom. With the kerf on top surface, the maximum width is 796 μm when the process is conducted with 3100W, and the minimum width of the kerf bottom is 375 μm at 3100W. As mentioned, the difference between top and bottom can be caused by various reasons, such as loss of intensity of the beam, defocusing of the laser beam, or loss of gas pressure for the thickness of the materials. In addition, as the laser power increases, a higher E_{line} is induced, and the kerf width cut by the high thermal energy increases. Each kerf width is observed to increase with increasing E_{line}. Therefore, the specimen is heavily influenced by the laser beam and rapidly heats up to the vaporization temperature of the material. Thus, the kerf width formed on the top surface is wider than that on the bottom surface.

3.4 Analysis of HAZ in SUS304 according to E_{line}

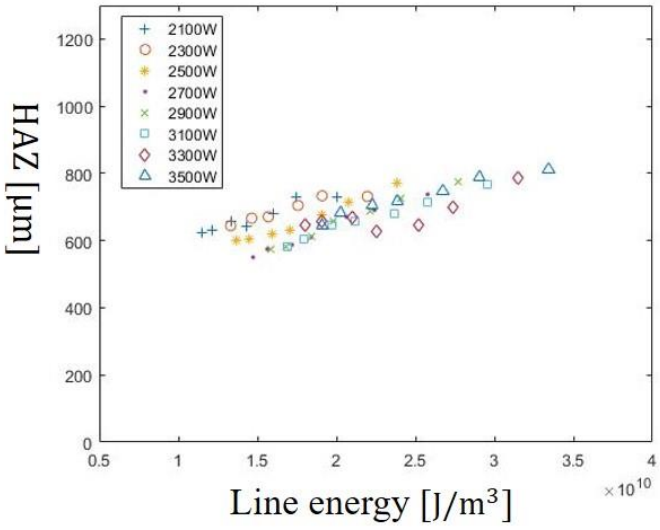

Figure 5 variation of the HAZ in SUS304 according to $\boldsymbol{E_{line}}$

The effects of the E_{line} on HAZ have been shown in Figure 5. HAZ is the area in which the microstructure of a material is changed by heat input. If the microstructure changes, a microcracks occurs in the processed material, it causes a partial breakdown of the product and deteriorates the quality. Therefore, it is important to reduce the HAZ so that micro cracks can be avoided in material processing quality. At the set laser parameter, the HAZ increased with increasing E_{line}. The maximum width of HAZ is 800 µm at 3500W and the minimum width of the HAZ is 550 µm at 2700 W. This can be related to the material ability to conduct heat. As the cutting speed increase, the time for heat conduction is lowered and the spread of heat damage is reduced in the material. Therefore, in order to reduce the HAZ of the materials processed with laser, HAZ can be reduced by reducing the size of the set laser power or cutting the cutting speed.

3.5 Multiple regression

In this section, the regression analysis of laser power and cutting speed in the laser cutting process is performed. Multiple regression analysis is a mathematical model for indicating the suitability of independent and dependent variable relationships. The regression equation used in this study is a quadratic regression model and the equation for the regression model is followed by:

$$y = \beta_0 + \sum_{i=1}^{n} \beta_i X_i + \sum_{i=1}^{n} \beta_{ii} X_i^2 + \sum_{i<j}^{n} \beta_{ij} X_i X_j \quad (2)$$

Where, β is the regression coefficient and can be calculated using least-squares method, X_i and X_j are the independent variables of this regression equation and these are laser power and cutting speed, respectively, y is the dependent variable and represents the data of each experiment. The second-order regression model is used for kerf top width, kerf bottom width, melting width, and HAZ using data from the experiments. To calculate the regression coefficient β, the coefficients of the quadratic regression model is calculated using MATLAB because a very complex relationship must be calculated. In addition, the determination coefficient R-value and the adjusted determination coefficient R_{adj} are calculated to check whether the data predicted by the regression model is appropriate. Regression coefficients are determined by the t-test, and each term is tested the null hypothesis according to the p-value. In general, P-values indicated lower than 0.05 can reject the null hypothesis and it can be considered significant for regression coefficients. Regression coefficient suitability and coefficient of determination are shown in Table 3.

$kerf_{top}$	Coefficient	SE Coef	T statistic	P-value
β_0	388.6832	80.07202	4.85417	8.75E-06
β_1	0.265692	0.033199	8.00299	4.35E-11
β_2	-0.00855	0.044628	-0.1916	0.848694
β_3	-3E-05	6.2E-06	-4.87501	8.11E-06
β_4	-8.5E-07	7.18E-06	-0.1179	0.906538
β_5	-7.6E-06	7.02E-06	-1.08053	0.28416

R-sq=0.90 R-sq(adj) = 0.89

$kerf_{bottom}$	Coefficient	SE Coef	T statistic	P-value
β_0	-5.9334786	89.49774223	-0.066297523	0.947357769
β_1	0.250301686	0.037857046	6.611759502	1.0722E-08
β_2	0.072250291	0.05112402	1.413235703	0.16266912
β_3	-3.28946E-05	7.25866E-06	-4.531773519	2.7836E-05
β_4	-1.37169E-05	8.75522E-06	-1.566708952	0.122356105
β_5	6.35527E-06	8.60318E-06	0.738711082	0.462915371

R-sq=0.89 R-sq(adj) = 0.88

melting	Coefficient	SE Coef	T statistic	P-value
β_0	1030.875039	112.6616	9.150191	4.76E-13
β_1	0.217366341	0.046711	4.653414	1.81E-05
β_2	-0.454709607	0.062792	-7.24157	8.9E-10
β_3	-7.9947E-06	8.73E-06	-0.91606	0.363242

β_4	8.18392E-05	1.01E-05	8.104238	2.91E-11
β_5	-2.86541E-05	9.88E-06	-2.8996	0.005187
R-sq=0.86 R-sq(adj) = 0.85				

Table 3 Regression coefficient of SS41

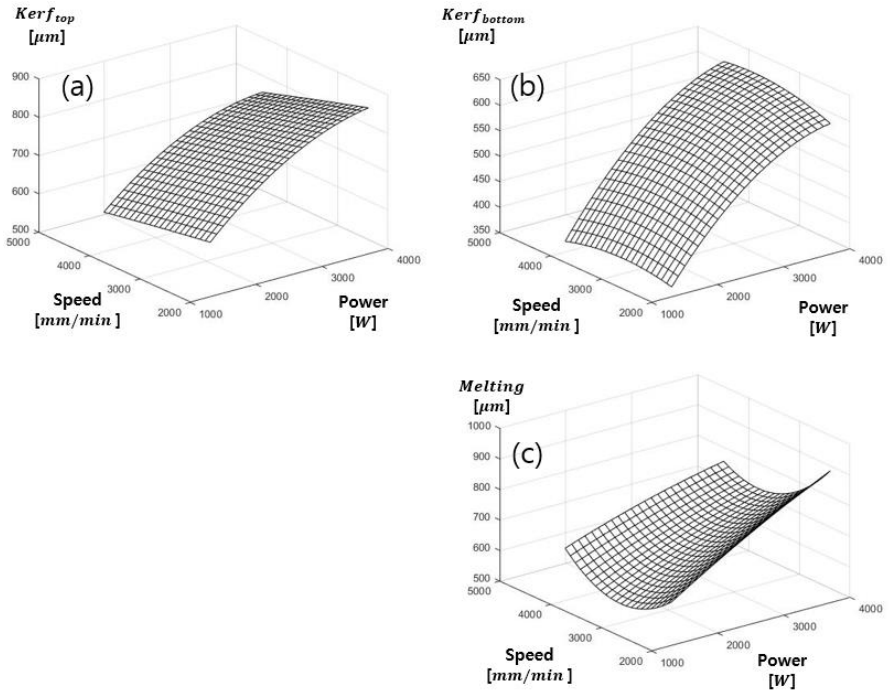

Figure 6 Multiple regress of SS41 (a) $\boldsymbol{kerf_{top}}$ (b) $\boldsymbol{kerf_{bottom}}$ (c) Melting

The regression model for kerf widths and melting width on SS41 is shown in Figure 6. Figure 6 (a) shows the regression model obtained from $kerf_{top}$. R_{sq} and $R_{sq}(adj)$ of the kerf top is 0.90 and 0.89, respectively, which is the experimental data are suitable for regression modeling. It also shows the most appropriate coefficient of determination among the regression models. In the relationship

between laser power and cutting speed, $\mathrm{kerf_{top}}$ is widely formed as the laser power increases and the cutting speed decreases. Figure 6 (b) shows the regression model obtained from $\mathrm{kerf_{bottom}}$. R_{sq} and R_{sq}(adj) of $\mathrm{kerf_{bottom}}$ were 0.89 and 0.88, which is the regression model was appropriate for the experimental data. In the effect of laser power and cutting speed on $\mathrm{kerf_{bottom}}$, it is widely formed according to changing the laser power. The regression model for melting width is shown in Figure 6 (c). In the case of the melting width, R_{sq} and R_{sq}(adj) were 0.86 and 0.85, respectively, which indicates that the regression model and the experimental data are suitable. In addition, the melting width decreases rapidly with decreasing laser power. In the case of cutting speed, a low melting width appears at around 3000mm / min.

185

$kerf_{top}$	Coefficient	SE Coef	T statistic	P-value
β_0	853.0468	251.3251	3.394196	0.001371
β_1	0.167979	0.129446	1.297679	0.200474
β_2	-0.21867	0.11114	-1.96752	0.054797
β_3	-1.1E-06	2.14E-05	-0.05021	0.960161
β_4	4.6E-05	1.84E-05	2.498231	0.015886
β_5	-5E-05	1.76E-05	-2.82229	0.006871

R-sq=0.80, R-sq(adj) = 0.78

$kerf_{bottom}$	Coefficient	SE Coef	T statistic	P-value
β_0	-108.267	69.11328	-1.56651	0.123665
β_1	0.360518	0.035597	10.12777	1.32E-13
β_2	-0.05506	0.030563	-1.8015	0.077778
β_3	-5.3E-05	5.9E-06	-8.97845	6.35E-12
β_4	8.64E-06	5.06E-06	1.707061	0.094141
β_5	-8.1E-06	4.83E-06	-1.67321	0.100659

R-sq=0.92 R-sq(adj) = 0.91

HAZ	Coefficient	SE Coef	T statistic	P-value
β_0	2289.716	218.9419	10.4581	4.46E-14
β_1	-0.68795	0.112767	-6.10062	1.64E-07
β_2	-0.40922	0.09682	-4.22663	0.000103

β_3	0.000132	1.87E-05	7.041524	5.72E-09
β_4	6.28E-05	1.6E-05	3.913384	0.000281
β_5	-1.4E-05	1.53E-05	-0.91761	0.363319
R-sq=0.85 R-sq(adj) = 0.83				

Table 4 Regression coefficient of SUS304

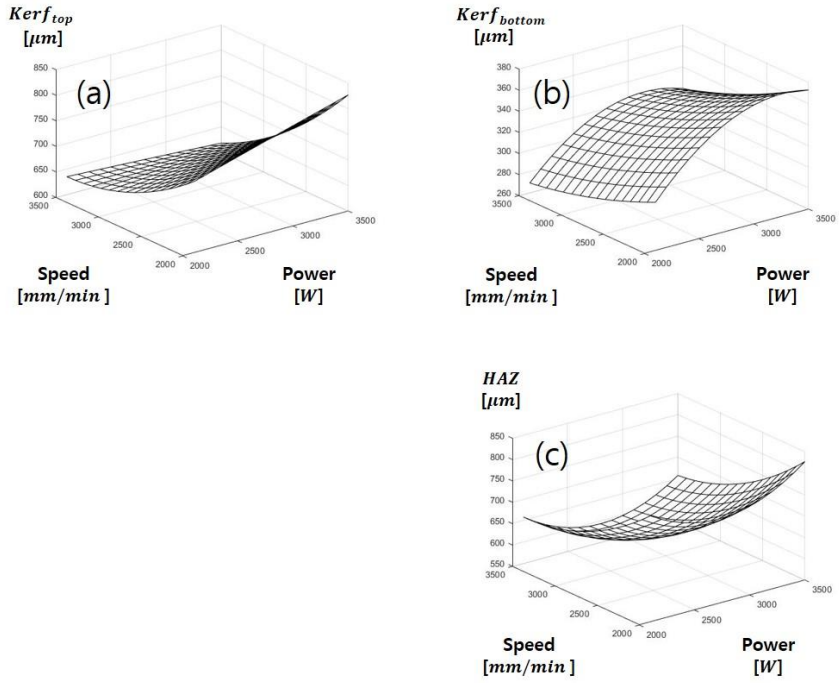

Figure 7 Multiple regress of SUS304 (a) $\boldsymbol{kerf_{top}}$, (b) $\boldsymbol{kerf_{bottom}}$, (c) HAZ

The regression model for kerf widths and HAZ on SUS304 is shown in Figure 7. Regression results for $kerf_{top}$ represent that R-sq and R-sq (adj) are 0.80 and 0.78, respectively. It is also determined that experimental data and regression modeling are relatively suitable. In the relation

between laser power and cutting speed, the higher the laser power and the lower the cutting speed induces the wider $\mathrm{kerf_{top}}$. This means that the amount of energy irradiated to the material increase according to increased laser power and decrease cutting speed. The regression model of $\mathrm{kerf_{bottom}}$ is suitable for experimental data with R_{sq} = 0.89 and R_{sq}(adj) = 0.88. It shows the most appropriate decision coefficient among the regression models for SUS304. In the regression model for the HAZ, the R_{sq} and R_{sq}(adj) of the coefficients of determination are 0.85 and 0.83, respectively, which are in good agreement with the experimental results. As the cutting speed decreases, the HAZ width increases rapidly, and the lower tendency of HAZ irradiated with set range of laser power is predicted at the cutting speed around 3000mm / min.

3.5 ANOVA

The analysis of variance (ANOVA) is shown in Table 5. ANOVA statistically analyzes the effect of each independent variable on the dependent variable during laser cutting. The advantage of ANOVA can identify important factors for each independent variable, as well as the interaction effect of each parameter on laser cutting quality. The variability of the experimental data can be determined by the contribution rate (PCR) of each independent variable. In addition, the results of the ANOVA are represented by the 95% confidence level ($P \leq 0.05$) and it is considered that the independent variable has a statistically significant effect on the experimental data. Table 5 and Table 6 for ANOVA results show kerf top, kerf bottom, melting and HAZ of Degrees of Freedom (DF), Sum of Squares (SS), Mean squares (MS), and contribution In the results of ANOVA, the P-value on the effect of each parameter and interaction is less than 0.05. This indicates that the parameters used have a significant effect on the experimental results.

The ANOVA results for SS41 are shown in Table 5. In each ANOVA Table, the results of kerf_{top}, $\text{kerf}_{\text{bottom}}$, melting width, and HAZ for 95% confidence level ($P < 0.05$) show significant influence on each material in the set parameters. In the kerf_{top} of SS41, it shows that the most effective variables in the kerf_{top} of the SS41 is laser power which is 59.28% of the percentage of the contribution (PCR). The other variables affecting kerf_{top} are cutting speed and laser power $*$ cutting speed at 12.48 % and 27.99 % respectively. In the results of ANOVA on the $\text{kerf}_{\text{bottom}}$, the laser power is the most effective variables which is 73.06 % of percentage of contribution (PCR). The other variables affecting $\text{kerf}_{\text{bottom}}$ are cutting speed and laser power $*$ cutting speed at 5.63 % and 20.37 % respectively. The most effective variable for melting width is laser power, with 59.65%

PCR. Also, the PCR of the cutting speed and laser power * cutting speed were 12.08% and 27.35%, respectively.

The ANOVA results for SUS304 are shown in Table 6. In the case of $\mathrm{kerf}_{\mathrm{top}}$ on SUS304, the most effective variables in laser power * cutting speed is 78.33% of PCR. In the ANOVA results of laser power and cutting, speed, the PCR is 9.93% and 10.45% respectively. In the variables affecting $\mathrm{kerf}_{\mathrm{bottom}}$, laser power * cutting speed and laser power have similar effects on the $\mathrm{kerf}_{\mathrm{bottom}}$. PCR of laser power * cutting speed and laser power showed 40.25% and 38.3%, respectively. In the results of HAZ, the interaction effect of the laser power * cutting speed is the most effective variable, 40.78 of PCR.

Source	SS	DF	MS	F ratio	P	PCR
$\mathrm{kerf}_{\mathrm{top}}$						
Laser Power	5627420.61	8.00	703427.58	4172.00	<0.05	59.28
Cutting Speed	1184668.18	7.00	169238.31	1003.75	<0.05	12.48
Laser power * Cutting speed	2657200.55	56.00	47450.01	281.42	<0.05	27.99
Error	24279.36	144.00	168.61			0.26
Total	9493568.70	215.00				
$\mathrm{kerf}_{\mathrm{bottom}}$						
Laser Power	3990213.86	8.00	498776.73	1400.60	<0.05	73.06
Cutting Speed	307606.70	7.00	43943.81	123.40	<0.05	5.63
Laser power * Cutting speed	1112774.73	56.00	19870.98	55.80	<0.05	20.37
Error	51280.85	144.00	356.12			0.94
Total	5461876.14	215.00				
Melting						
Laser Power	5279848.53	8.00	659981.07	1163.22	<0.05	59.65
Cutting Speed	1069208.64	7.00	152744.09	269.21	<0.05	12.08
Laser power * Cutting speed	2421142.11	56.00	43234.68	76.20	<0.05	27.35
Error	81701.86	144.00	567.37			0.92
Total	8851901.13	215.00				

234 *Table 5 SS41 ANOVA table*

235

236

Source	SS	DF	MS	F ratio	P	PCR
$kerf_{top}$						
Laser Power	90451.73	9	10050.19	119.36	<0.05	9.93
Cutting Speed	95165.87	6	15860.98	188.37	<0.05	10.45
Laser power * Cutting speed	713458.15	54	13212.19	156.91	<0.05	78.33
Error	11788.16	140	84.20			1.29
Total	910863.92	209				
$kerf_{bottom}$						
Laser Power	185845.57	9	20649.51	389.47	<0.05	38.03
Cutting Speed	98838.53	6	16473.09	310.70	<0.05	20.22
Laser power * Cutting speed	196764.70	54	3643.79	68.73	<0.05	40.25
Error	7422.73	140	53.02			1.52
Total	488871.52	209				
HAZ						
Laser Power	602569.43	9	66952.16	43.07	<0.05	22.39
Cutting Speed	773417.99	6	128903.00	82.91	<0.05	28.74
Laser power * Cutting speed	1097317.73	54	20320.70	13.07	<0.05	40.78
Error	217654.36	140	1554.67			8.09

	Total	2690959.52	209

237 *Table 6 SUS304 ANOVA table*

238

4. Conclusion

The influences of the laser parameter such as laser power and cutting speed on the SS41 and SUS304 are studied in this experiment. The experiment results of laser cutting on different materials are analyzed through multiple regression and analysis of variance (ANOVA). The effects of each independent variable to output variables and the effect on the between independent variables to output variables are analyzed. The conclusion of this experiment is as follows:

1. We confirmed that the experimental results depend on the set laser parameters. From the experimental results according to E_{line}, the kerf width, melting width, and HAZ increases as the E_{line} increases. E_{line} is calculated with laser power and cutting speed. Therefore, the experimental results on laser cutting can be controlled by laser power and cutting speed.

2. In the case of multiple regression on the SS41 and SUS304, it is founded that the experimental results in kerf widths, melting, and HAZ are affected by set laser parameters. The effect of laser power and cutting speed is analyzed through the multiple regression model. The regression equation used in the analysis can appropriately predict output variables from independent variables. Besides, the coefficient of determination (R^2) for kerf widths and melting for SS41 are 0.89, 0.88 and 0.85, respectively. For the SUS304, the coefficients of determination for kerf widths and HAZ are 0.78, 0.91, 0.83 respectively.

3. The results of the ANOVA on the SS41 and SUS304 analyze the effect of each independent variable on the dependent variable during laser cutting. The most effective variables in kerf widths and melting width in SS41is laser power and the percentage of contribution (PCR) is 59.28 %, 73.06 %, and 59.65 %, respectively. In the case of $kerf_{top}$ on the SUS304, the most

effective variables in cutting speed is 78.33 % of PCR. On the other hand, for the $\mathrm{kerf}_{\mathrm{bottom}}$ and HAZ, the interaction effects of the laser cutting speed $*$ cutting speed have been found most effective variables of the 40.25 % and 40.78 %, respectively.

Acknowledgement

The research described herein was sponsored by the National Research Foundation of Korea (NRF) grant funded by the Korean government (MSIP; Ministry of Science, ICT & Future planning) (No. 2019R1A2C1089644). The opinions expressed in this paper is those of the authors and do not necessarily reflect the views of the sponsors.

Reference

1. Rajaram, N., J. Sheikh-Ahmad, and S. Cheraghi, *CO2 laser cut quality of 4130 steel.* International Journal of Machine Tools and Manufacture, 2003. **43**(4): p. 351-358.
2. Lee, D., Y. Seo, and S. Pyo, *Effect of laser speed on cutting characteristics of cement-based materials.* Materials, 2018. **11**(7): p. 1055.
3. Wang, J. and W. Wong, *CO2 laser cutting of metallic coated sheet steels.* Journal of Materials Processing Technology, 1999. **95**(1-3): p. 164-168.
4. Lee, D. and S. Pyo, *Experimental Investigation of Multi-mode Fiber Laser Cutting of Cement Mortar.* Materials, 2018. **11**(2): p. 278.

5. Lee, D. and J. Mazumder, *Effects of momentum transfer on sizing of current collectors for lithium-ion batteries during laser cutting.* Optics & Laser Technology, 2018. **99**: p. 315-325.

6. Seo, Y., D. Lee, and S. Pyo, *Microstructural Characteristics of Cement-Based Materials Fabricated Using Multi-Mode Fiber Laser.* Materials, 2020. **13**(3): p. 546.

7. Lee, D., *Understanding of BeCu Interaction Characteristics with a Variation of ns Laser-Pulse Duration.* Materials, 2018. **11**(8): p. 1423.

8. Lee, D., *Investigation of Physical Phenomena and Cutting Efficiency for Laser Cutting on Anode for Li-Ion Batteries.* Applied Sciences, 2018. **8**(2): p. 266.

9. Lee, D. and J. Mazumder, *Dataset demonstrating effects of momentum transfer on sizing of current collector for lithium-ion batteries during laser cutting.* Data in brief, 2018. **17**: p. 6-14.

10. Lee, D. and S. Ahn, *Investigation of Laser Cutting Width of LiCoO2 Coated Aluminum for Lithium-Ion Batteries.* Applied Sciences, 2017. **7**(9): p. 914.

11. Lee, D., et al., *Application of laser spot cutting on spring contact probe for semiconductor package inspection.* Optics & Laser Technology, 2017. **97**: p. 90-96.

12. Lee, D., *Experimental investigation of laser spot welding of Ni and Au-Sn-Ni alloy.* Journal of Welding and Joining, 2017. **35**(2): p. 1-5.

13. Lee, D., et al., *Three dimensional simulation of high speed remote laser cutting of cathode for lithium-ion batteries.* Journal of Laser Applications, 2016. **28**(3): p. 032010.

14. Lee, D., et al., *Parameter optimization for high speed remote laser cutting of electrodes for lithium-ion batteries.* Journal of Laser Applications, 2016. **28**(2): p. 022006.

15. Lamikiz, A., et al., *CO2 laser cutting of advanced high strength steels (AHSS).* Applied surface science, 2005. **242**(3-4): p. 362-368.

16. Kaebernick, H., A. Jeromin, and P. Mathew, *Adaptive control for laser cutting using striation frequency analysis.* CIRP Annals, 1998. **47**(1): p. 137-140.

17. Rajaram, N., J. Sheikh-Ahmad, and C. Hossein, *Parametric study of the effect of feed speed and power on laser cut quality of 4130 steel.* Wichita State University: Wichita, Kansas, 2002: p. 67260-0035.

18. Yilbas, B., *Effect of process parameters on the kerf width during the laser cutting process.* Proceedings of the Institution of Mechanical Engineers, Part B: Journal of Engineering Manufacture, 2001. **215**(10): p. 1357-1365.

19. Anghel, C., K. Gupta, and T. Jen, *Analysis and optimization of surface quality of stainless steel miniature gears manufactured by CO2 laser cutting.* Optik, 2020. **203**: p. 164049.

20. Lee, D., B. Oh, and J. Suk, *The Effect of Compactness on Laser Cutting of Cathode for Lithium-Ion Batteries Using Continuous Fiber Laser.* Applied Sciences, 2019. **9**(1): p. 205.

Figures

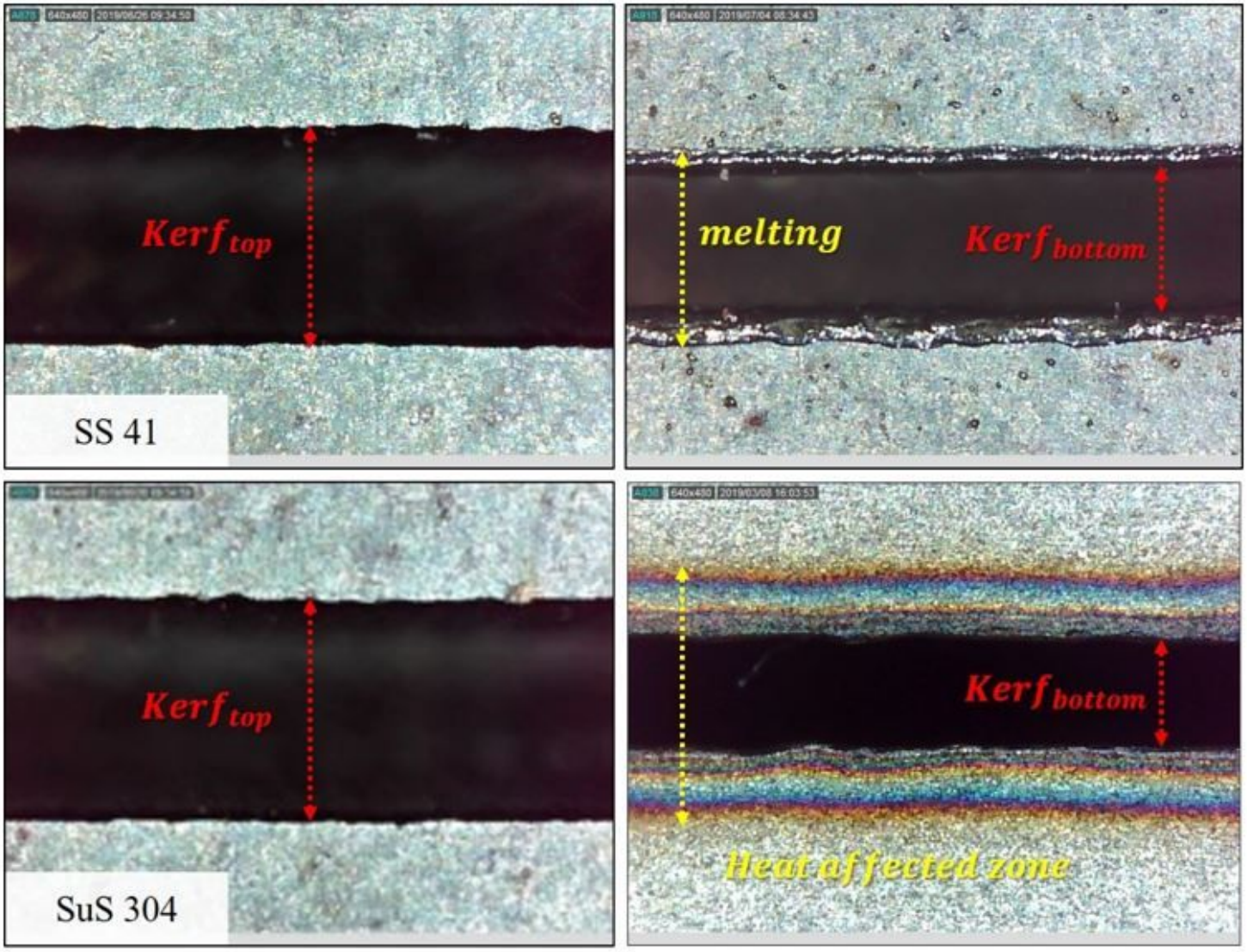

Figure 1

Measurement method

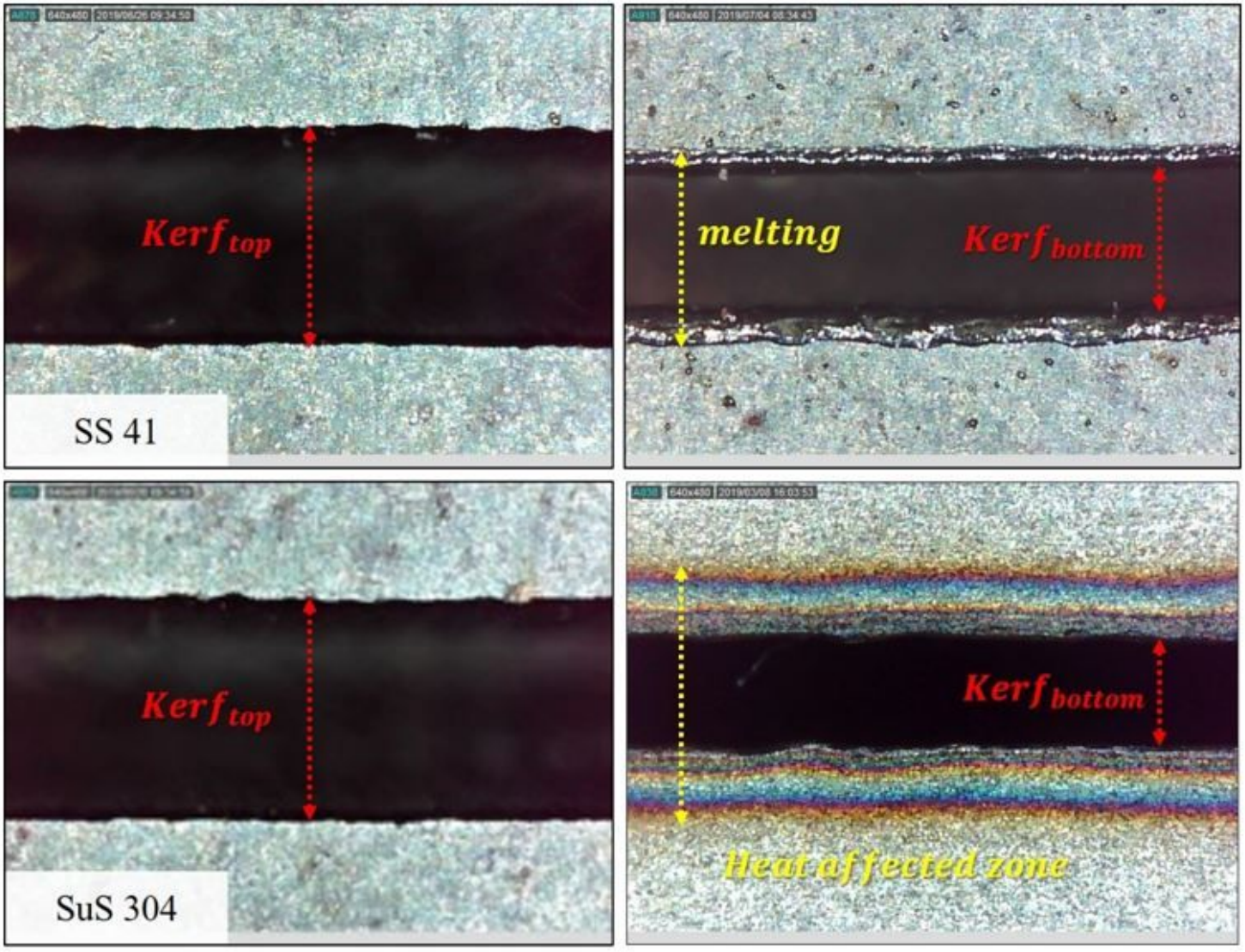

Figure 1

Measurement method

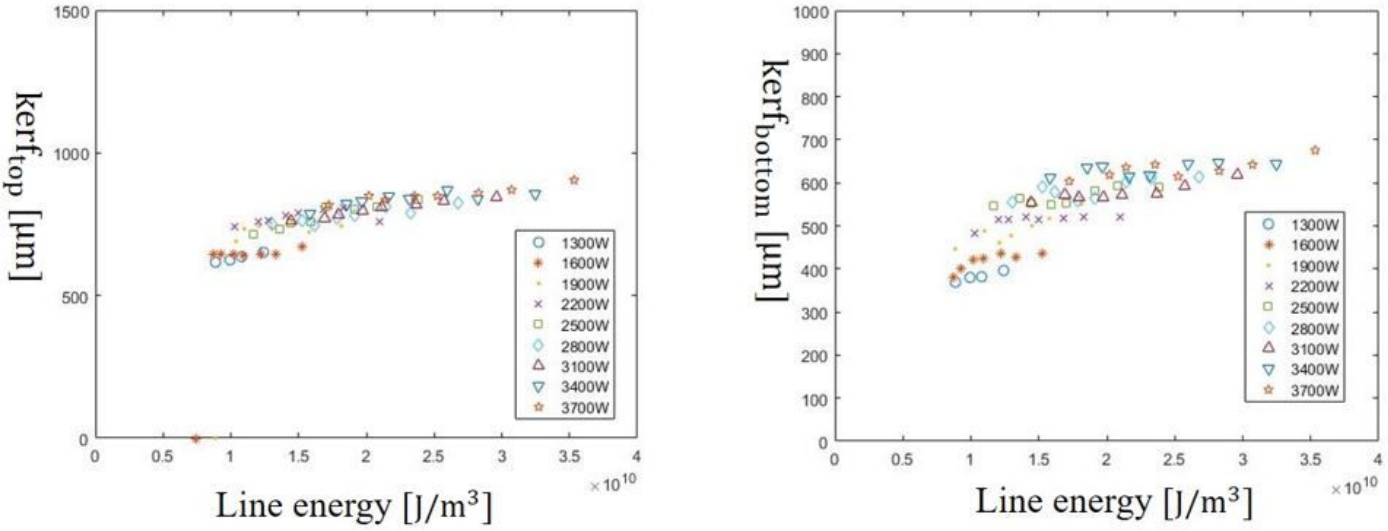

Figure 2

Variation of kerf_top and kerf_bottom according to E_line

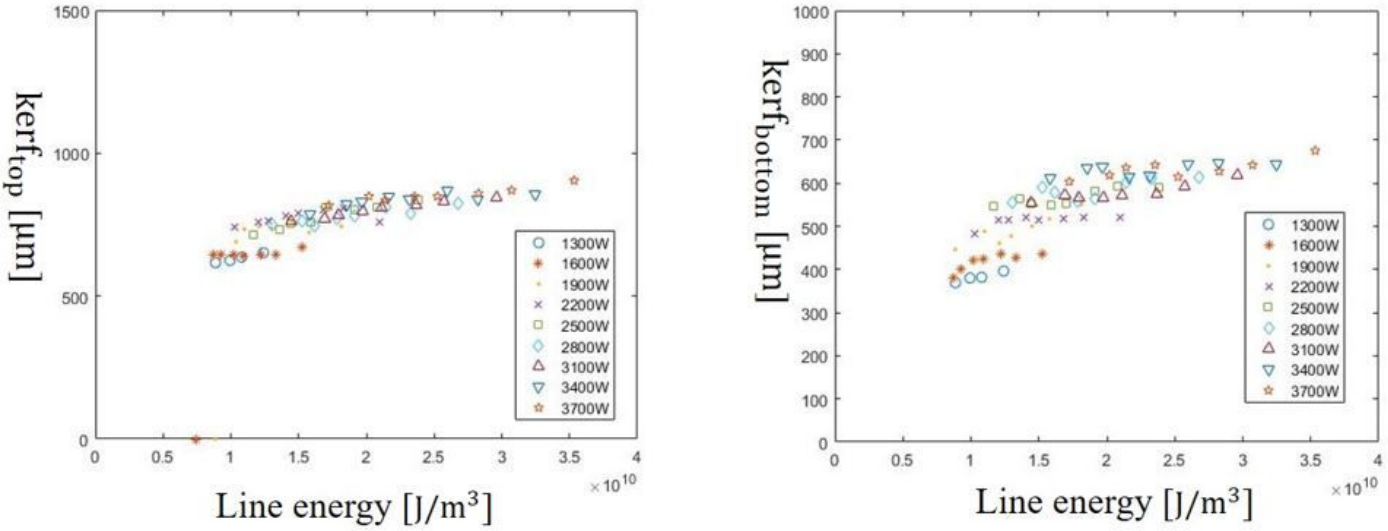

Figure 2

Variation of kerf_top and kerf_bottom according to E_line

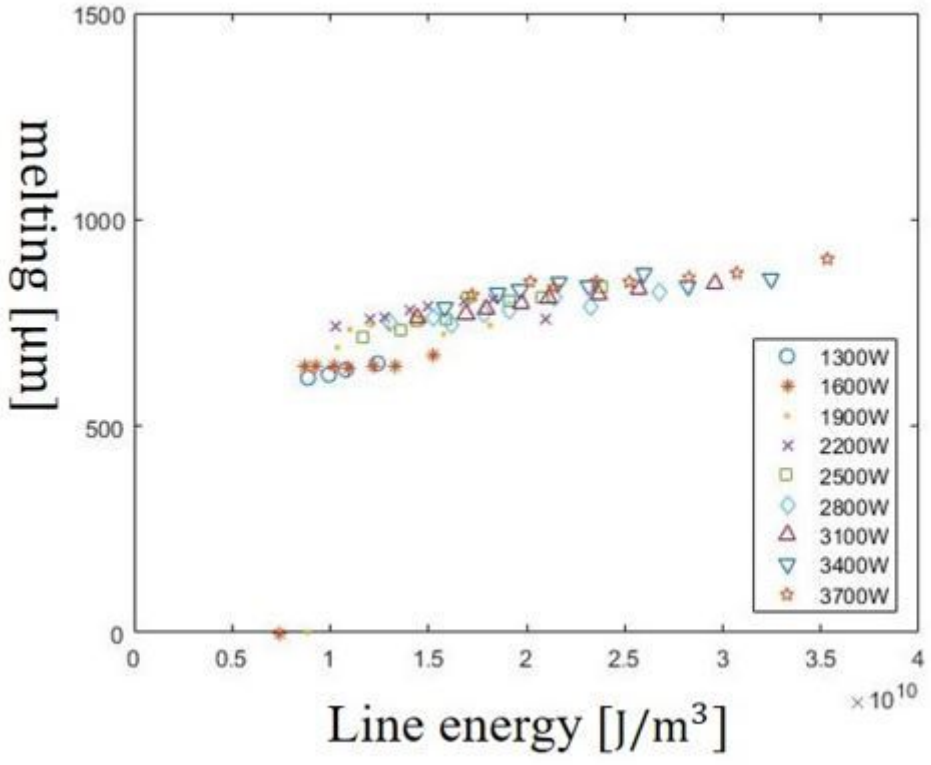

Figure 3

Variation of melting according to E_line

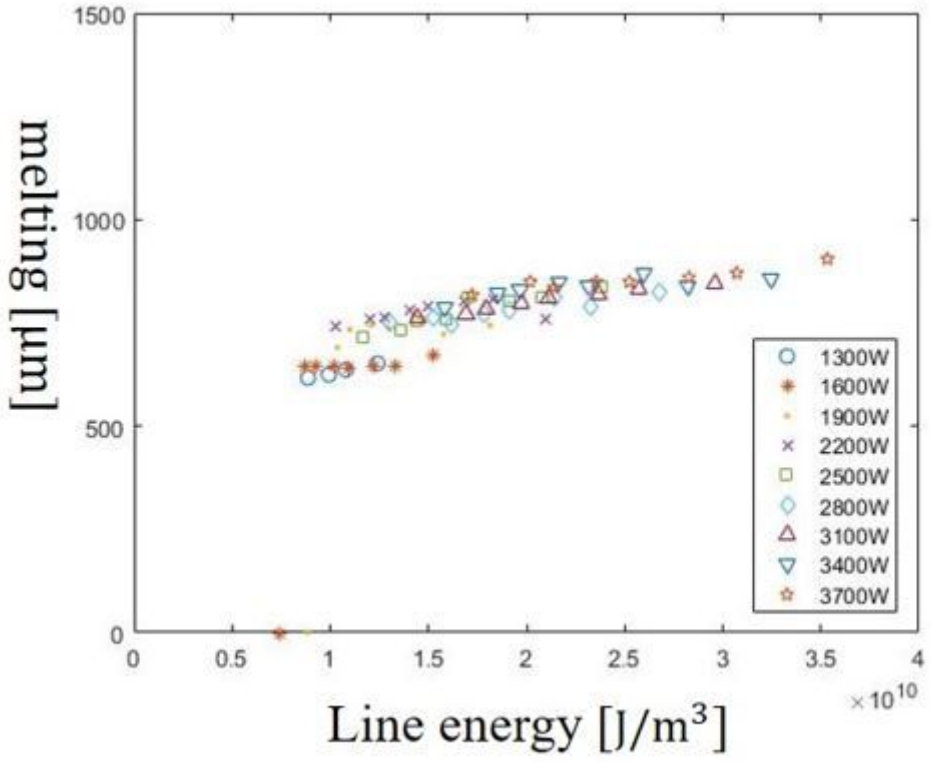

Figure 3

Variation of melting according to E_line

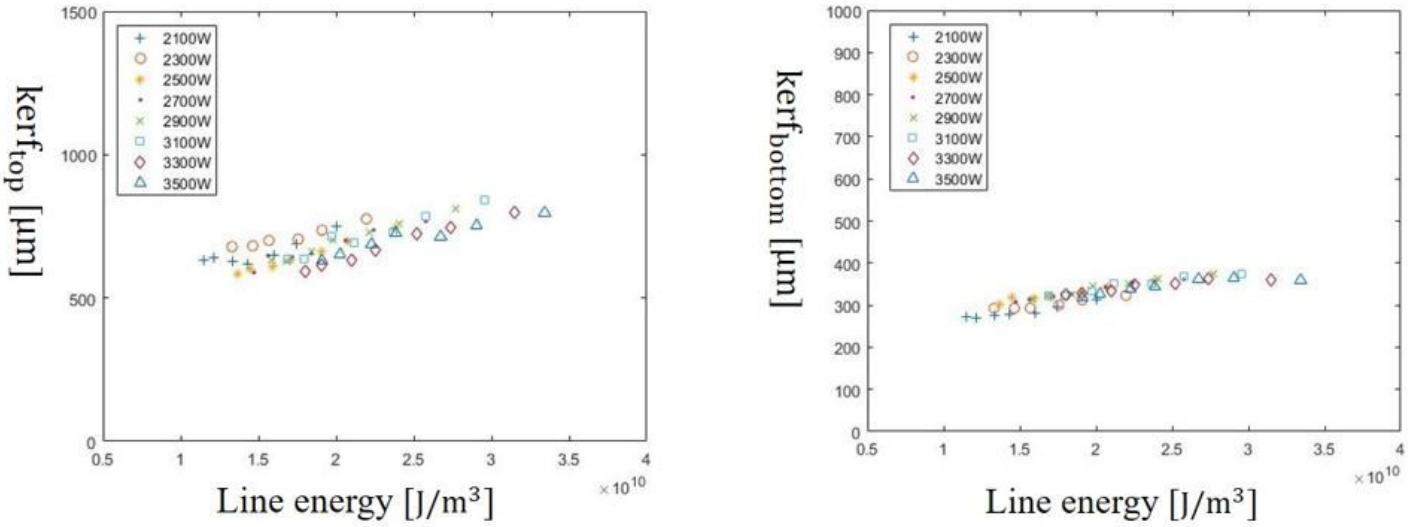

Figure 4

variation of kerf_top and kerf_bottom in SUS304 according to E

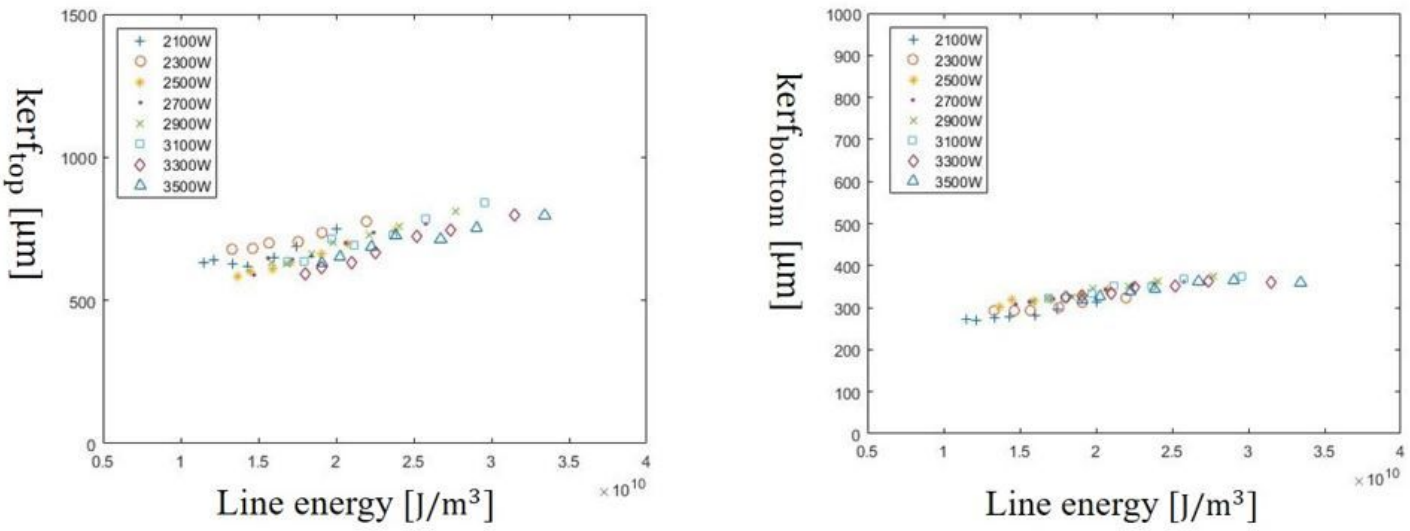

Figure 4

variation of kerf_top and kerf_bottom in SUS304 according to E

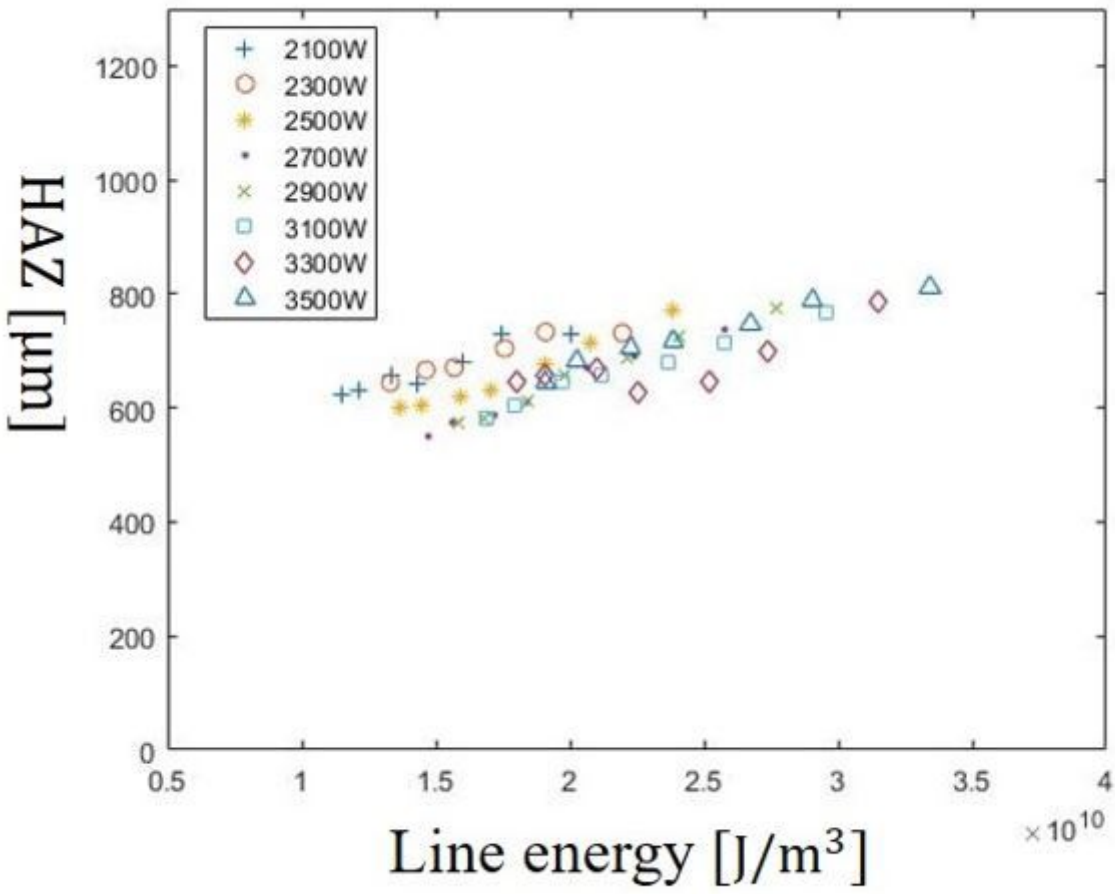

Figure 5

variation of the HAZ in SUS304 according to E_line

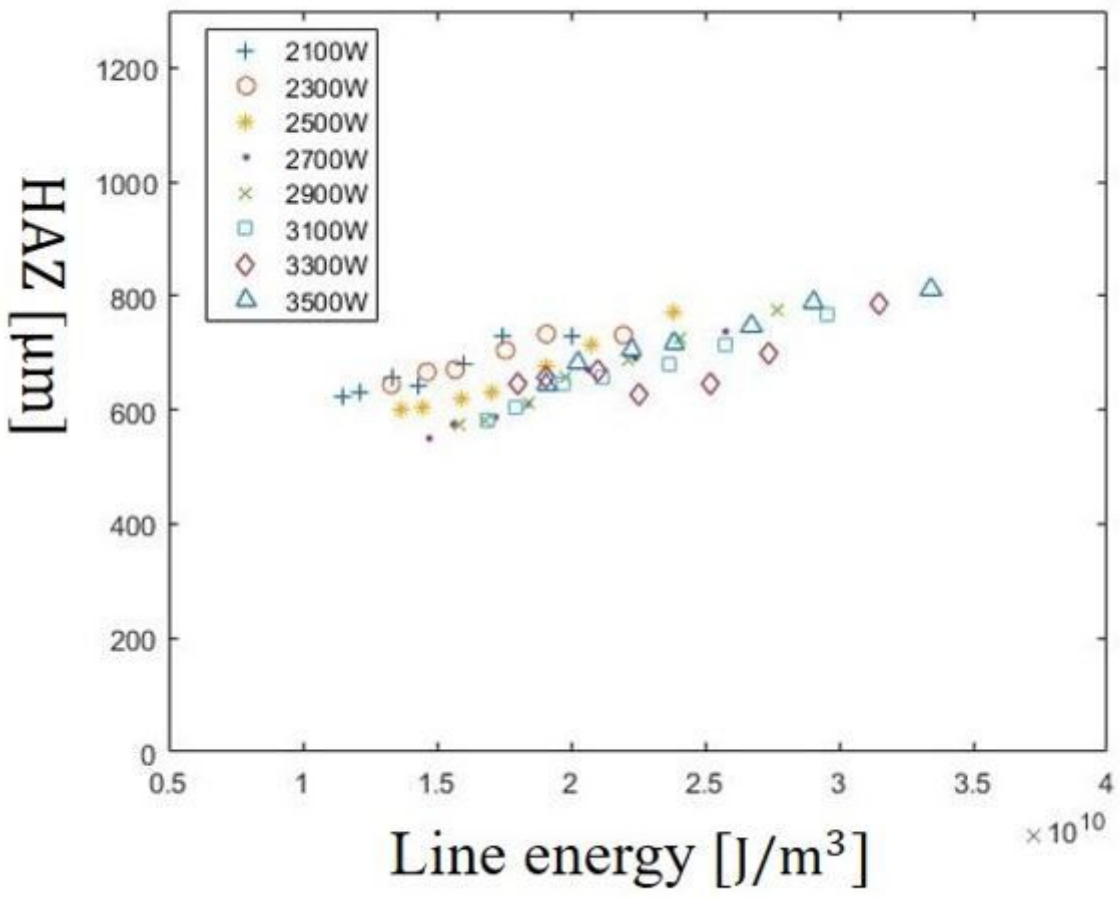

Figure 5

variation of the HAZ in SUS304 according to E_line

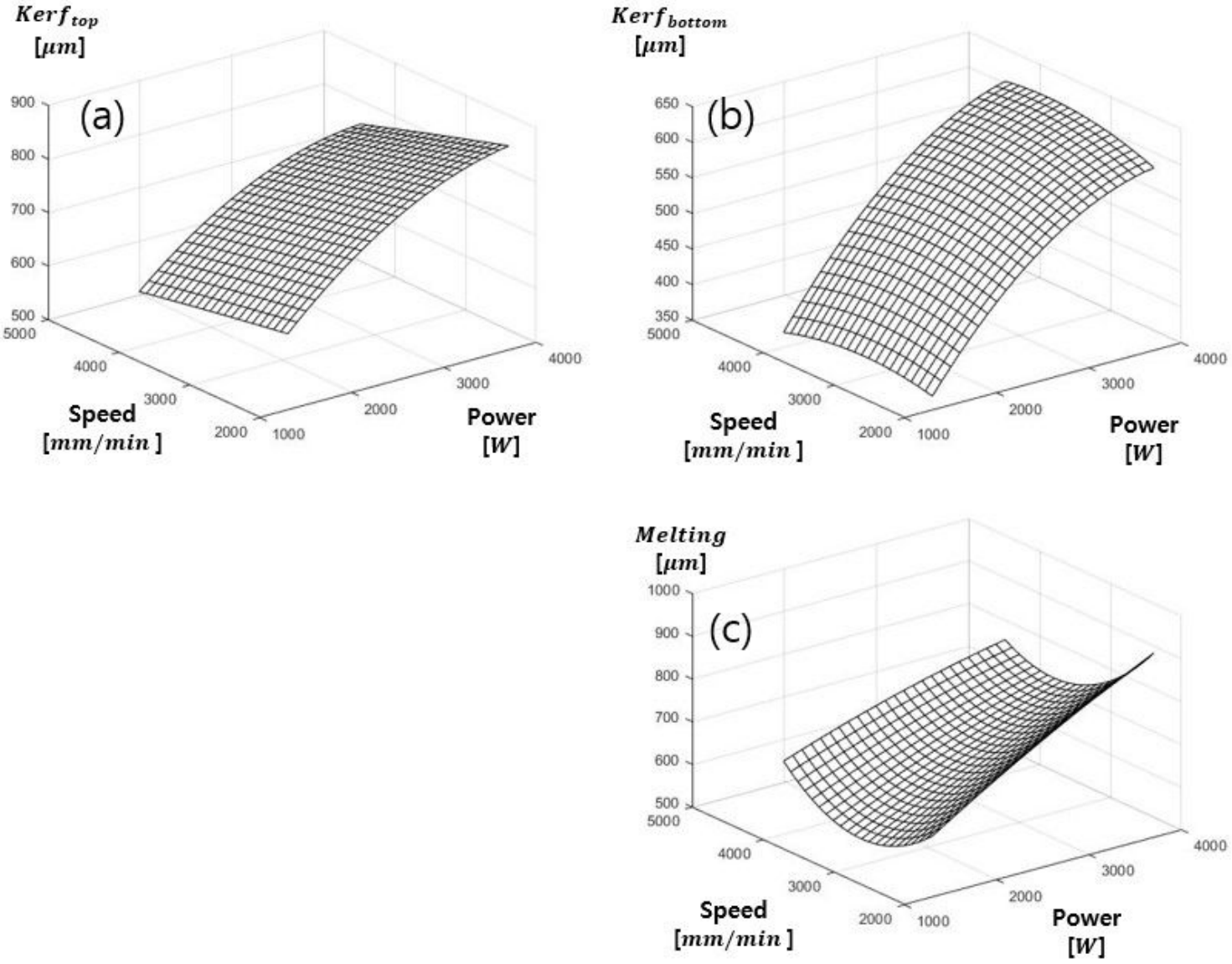

Figure 6

Multiple regress of SS41 (a) kerf_top (b) kerf_bottom (c) Melting

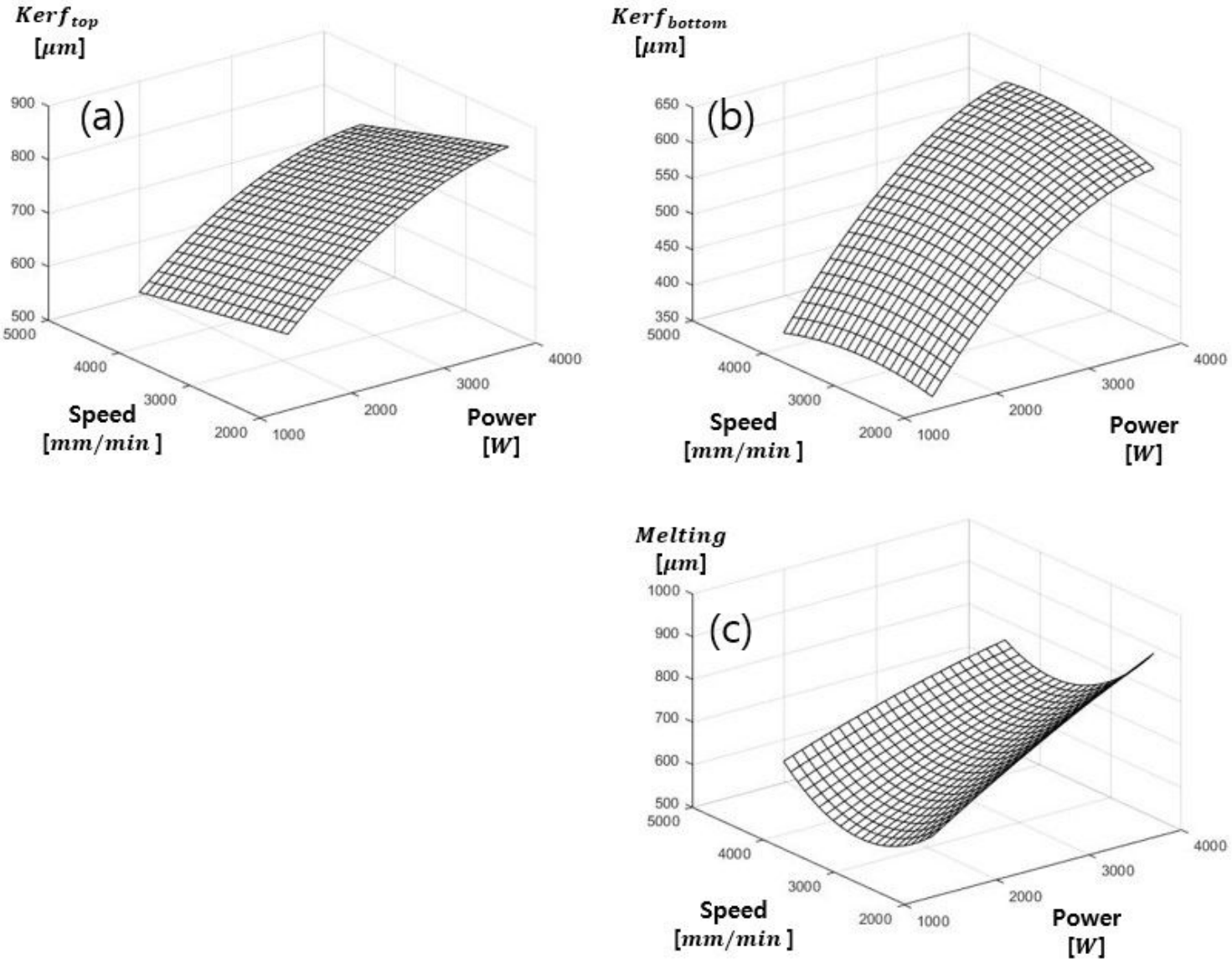

Figure 6

Multiple regress of SS41 (a) kerf_top (b) kerf_bottom (c) Melting

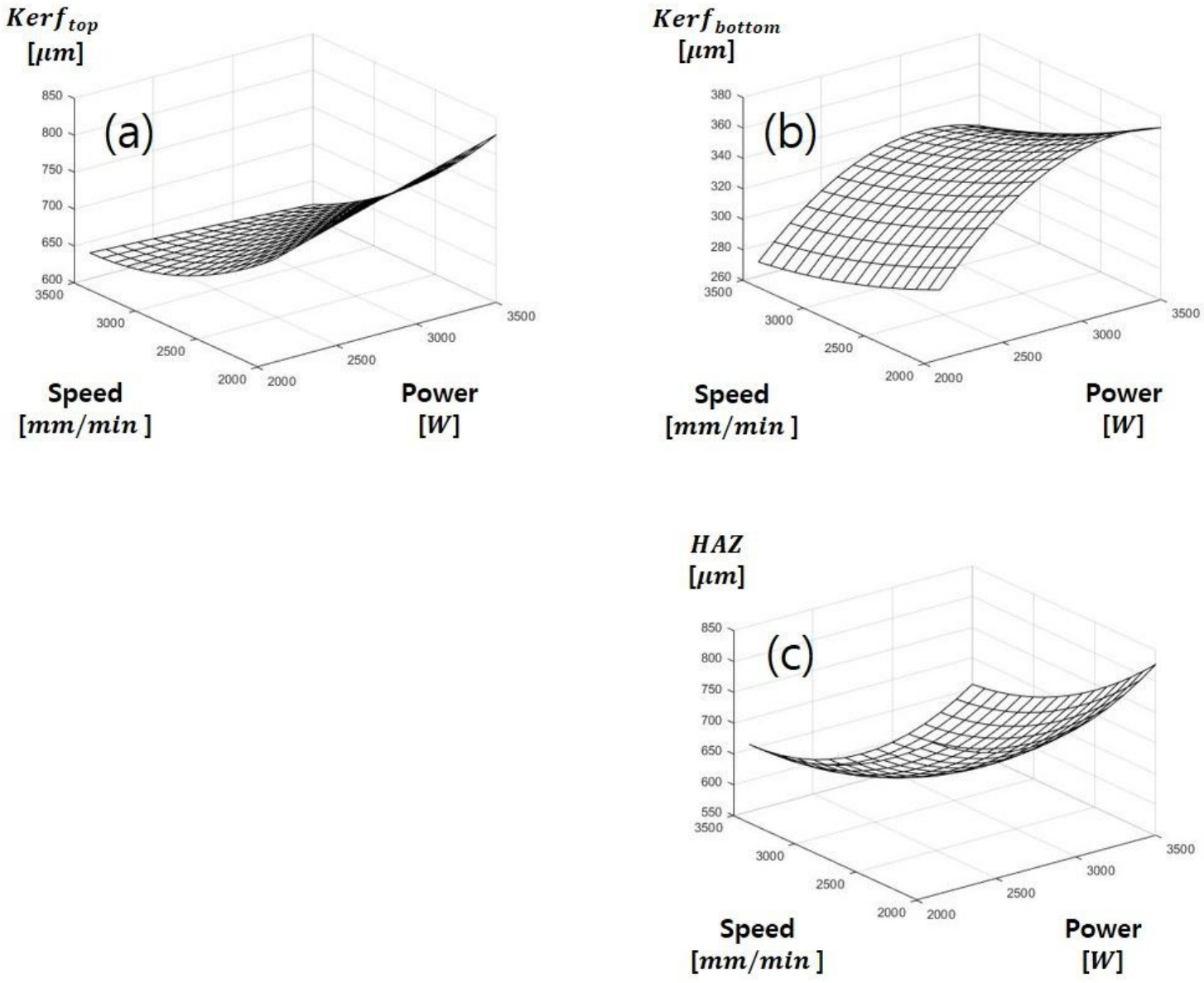

Figure 7

Multiple regress of SUS304 (a) kerf_top, (b) kerf_bottom, (c) HAZ

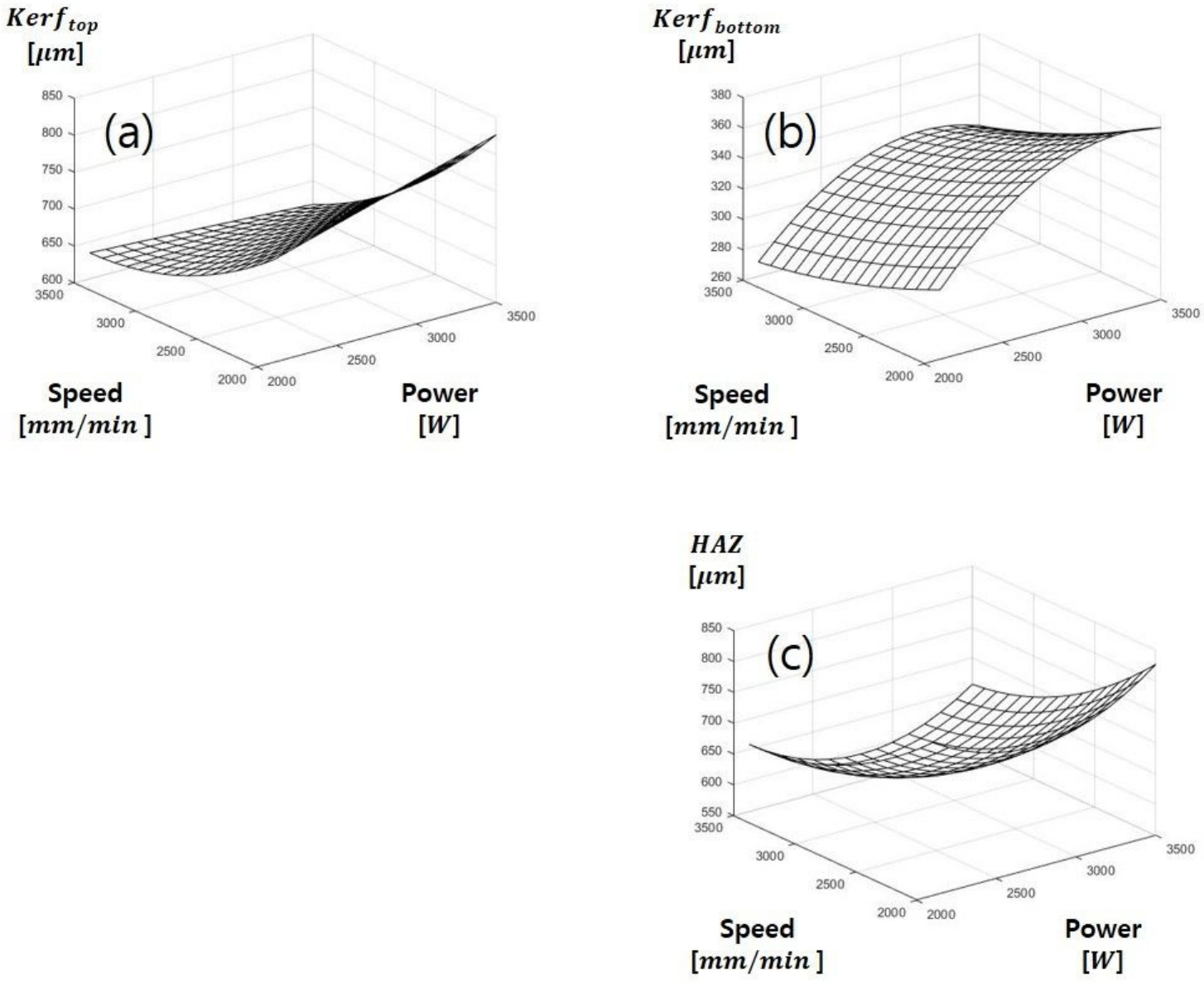

Figure 7

Multiple regress of SUS304 (a) kerf_top, (b) kerf_bottom, (c) HAZ